8

Application of Radar Technology to Deflection Measurement and Dynamic Testing of Bridges

Carmelo Gentile
Politecnico di Milano, Dept. of Structural Engineering
Italy

1. Introduction

Vibration testing of bridges and large structures is generally performed by using piezoelectric or force-balanced accelerometers since these sensors are very accurate and relatively inexpensive. Although accelerometers have been – and still are – extensively and successfully used, their drawbacks are well-known: (1) the sensors must be installed at selected locations that are representative of the structure motion and access may be difficult and often dangerous; (2) the installation and wiring are the most time-consuming tasks during the tests; (3) the use in permanent monitoring systems is prone to the typical failures of any system provided with cables and electrical circuits; and (4) accelerometers do not provide a direct measurement of displacement, something that could positively affect the development of the Structural Health Monitoring (SHM) in operational conditions.
Within this context, the development of innovative non-contact systems for vibration measurement is very attractive and especially applications of laser-based systems (Cunha & Caetano 1999, Kaito *et al.* 2005) are reported in the literature. Other recent investigations suggest the application of Global Positioning Systems (GPS, Nickitopoulou *et al.* 2006, Meng *et al.* 2007) or image analysis and vision systems (Lee *et al.* 2006, Silva *et al.* 2007). Furthermore, a non-contact system using microwaves was described by Farrar *et al.* (1999) and used to measure the vibration response of the well-known I-40 bridge over Rio Grande river (Farrar & Cone 1995); this sensor did not provide any *range resolution*, i.e. was not capable to detect different targets in the scenario illuminated by the microwave beam.
Recent progresses in radar techniques and systems have favoured the development of a microwave interferometer, potentially suitable to the non-contact vibration monitoring of large structures (Pieraccini *et al.* 2004, Bernardini *et al.* 2007, Gentile & Bernardini 2008, Gentile 2009). The main characteristic of this new radar system – entirely designed and developed by Italian researchers – is the possibility of simultaneously measuring the static or dynamic deflections of several points of a structure, with sub-millimetric accuracy. For the radar vibrometer, each discontinuity of a structure – such as the "corner zones" corresponding to the intersection of girders and cross-beams in the deck of bridges – represents a potential source of reflection of the electromagnetic waves generated by the radar; in such cases, an echo can be generated and the corner zones act as a series of virtual sensors. In addition to its non-contact feature, the sensor provides other advantages including a wide frequency range of response, portability and quick setup time.

Source: Radar Technology, Book edited by: Dr. Guy Kouemou,
ISBN 978-953-307-029-2, pp. 410, December 2009, INTECH, Croatia, downloaded from SCIYO.COM

The radar sensor detects the position and the displacement of target points placed at different distances from the equipment by using two well-known radar techniques: the Stepped-Frequency Continuous Wave (SF-CW, Wehner 1995) and the Interferometric techniques (Henderson & Lewis 1998).
This chapter first describes the basic principles implemented in the new sensor, its technical characteristics and the results of the laboratory tests carried out to evaluate the accuracy and the intrinsic performance of the equipment. Subsequently, the application to field test of different full-scale bridges is summarized and reviewed. The field tests include the measurement of vibration responses on structural elements very difficult to access by using conventional techniques, such as stay cables (Gentile 2009). During the presented experimental tests, the microwave interferometer and conventional accelerometers were simultaneously used; hence, the analysis of acquired signals included extensive comparison between the time series recorded by the radar and the accelerometers and the comparison clearly exemplifies the major advantages and drawbacks of the radar equipment. Furthermore, resonant frequencies and mode shapes of the investigated vibrating systems, that were identified from the radar signals, are compared to the corresponding quantities estimated from the accelerometer's records.

2. Radar techniques implemented in the microwave interferometer

The most peculiar and important characteristic of a conventional radar is its ability to determine the range (i.e. the distance) by measuring the time for the radar signal to propagate to the target and back. Although the name *radar* is derived from radio detection and ranging, a radar is capable of providing more information about the target than its name would imply. Typical applications (see e.g. Skolnik 1990) include the evaluation of the radial velocity, the angular direction, size and shape of the target.
The main functions of the new radar sensor herein described are the simultaneous detection of the position and deflection of different targets placed at different distances from the sensor. This performance is obtained by implementing two well-known radar techniques:

1. the Stepped-Frequency Continuous Wave technique (Wehner 1995), employed to detect the positions of different targets placed along the radar's line of sight;
2. the Interferometric technique (Henderson & Lewis 1998), implemented to compute the displacement of each target, by comparing the phase information of the back-scattered electromagnetic waves collected at different times.

2.1 The Stepped Frequency – Continuous Wave (SF-CW) technique

The usual radar waveform to determine the range is the short pulse. The shorter the pulse, the more precise is the measurement of the range because the range resolution Δr is related to the pulse duration τ by the following relationship:

$$\Delta r = \frac{c\tau}{2} \tag{1}$$

where c is the speed of light in free space. For a signal of duration τ, it can be shown (see e.g. Marple 1987) that the time-bandwidth product satisfies the equality $\tau B = 1$, where B is the equivalent bandwidth in Hz. Hence, the range resolution Δr may be expressed as:

$$\Delta r = \frac{c}{2B} \tag{2}$$

Eqs. (1) and (2) show that a better range resolution (corresponding to a smaller numerical value of Δr) can be obtained by either decreasing τ or increasing B. Instead of using short-time pulses, SF-CW radars exhibit a large bandwidth by linearly increasing the frequency of successive pulses in discrete steps, as shown in Fig. 1; hence, a SF-CW radar has a narrow instantaneous bandwidth (corresponding to individual pulse) and attains a large effective bandwidth:

$$B = (N-1)\Delta f \tag{3}$$

with a burst of N electromagnetic pulses, generally named tones, whose frequencies are increased from tone to tone by a constant frequency increment Δf.
In a SF-CW radar, the signal source dwells at each frequency $f_k = f_o + k\Delta f$ $(k=0,1,2, \ldots, N-1)$ long enough to allows the received echoes to reach the receiver. Hence, the duration of each single pulse (T_{tone}) depends on the maximum distance ($R_{\max}$) to be observed in the scenario:

$$T_{\text{tone}} = \frac{2R_{\max}}{c} \tag{4}$$

The number N of tones composing each burst can be computed as:

$$N = \frac{2R_{\max}}{\Delta r} \tag{5}$$

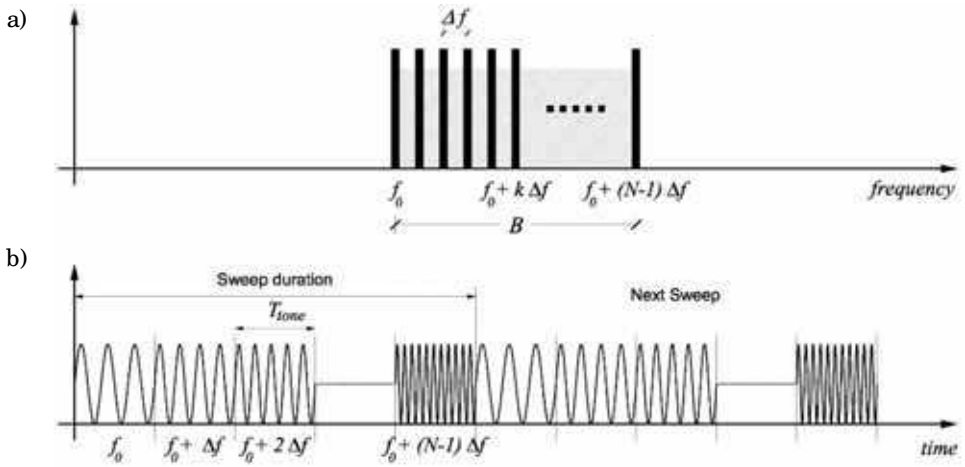

Fig. 1. Representation of SF-CW waveform in: a) frequency domain and b) time domain

The time scheduling (4) permits the SF-CW radar to receive the response of the furthest target before transmitting the following tone. On the other hand, eqs. (4)-(5) clearly highlight that the maximum sampling rate of the scenario f_{sample} depends on $R_{\max}$ and Δr. Specifically, accounting for eqs. (4)-(5), f_{sample} can be expressed as:

$$f_{\text{sample}} \cong \frac{1}{NT_{\text{tone}}} = \frac{c}{2NR_{\max}} = \frac{c\Delta r}{4R_{\max}^2} \tag{6}$$

Eq. (6) clearly shows that:

a. the maximum sampling rate decreases as the maximum measured distance increases (since the system has to wait for a longer time to receive the echo of the furthest target);
b. the maximum sampling rate increases as the range resolution increases.

The use of SF continuous waveform exhibits several advantages:

1. SF-CW radars can reach the same far distance of a pulse radar by transmitting lower power. In turn, low transmitted power generally allows SF-CW radars to be included in the Short-Range Device category as a license-free use equipment;
2. SF modulated radars can transmit and receive signals with precise frequency control by using Direct Digital Synthesizer (DDS), an innovative up-to-date device for generating SF waveforms.

SF waveforms produce a synthetic profile of scattering objects through the procedure summarized in Fig. 2. At each sampled time instant, both in-phase (I) and quadrature (Q) components of the received signals are acquired so that the resulting data consist of a vector of N complex samples, representing the frequency response measured at N discrete frequencies. By taking the Inverse Discrete Fourier Transform (*IDFT*), the response is reconstructed in the time domain of the radar: each complex sample in this domain represents the echo from a range (distance) interval of length $c/2B$. The amplitude range profile of the radar echoes is then obtained by calculating the magnitude of the *IDFT* of acquired vector samples.

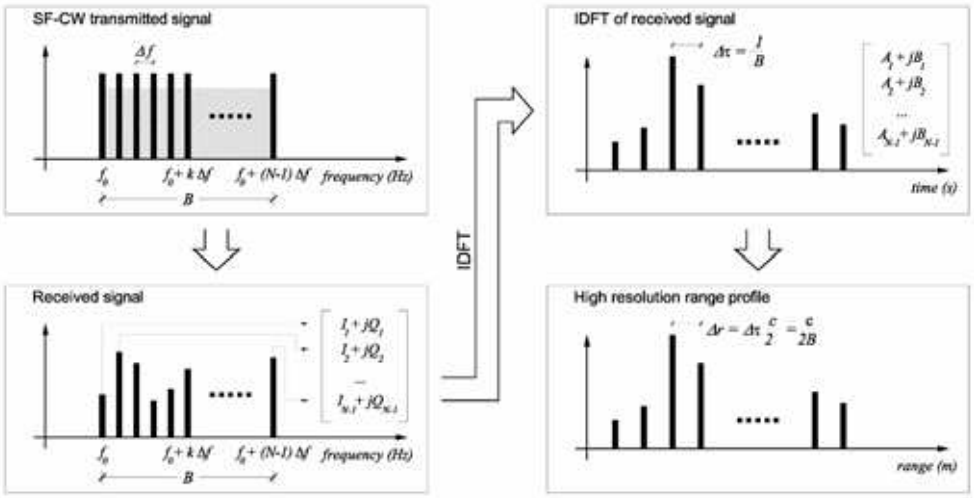

Fig. 2. Evaluation of high-resolution range profile from SF-CW waveform

The amplitude range profile gives a one-dimensional (1-D) map of the scattering objects in the space illuminated by the antenna beam, as a function of their relative distance from the sensor.

The concept of range profile is better illustrated in Fig. 3, where an ideal range profile is shown, as obtained when the radar transmitting beam illuminates a series of targets at

different distances and different angles from the axis of the system. The peaks in the plot of Fig. 3 correspond to points with good electromagnetic reflectivity: the sensor can simultaneously detect the displacement or the transient response of these points. Fig. 3 also shows that the radar has only 1-D imaging capabilities, i.e. different targets can be individually detected if they are placed at different distances from the radar. Hence, measurement errors may arise from the multiplicity of contributions to the same range bin, coming from different points placed at the same distance from the radar but not lying on the same axis (Gentile *et al.* 2008).

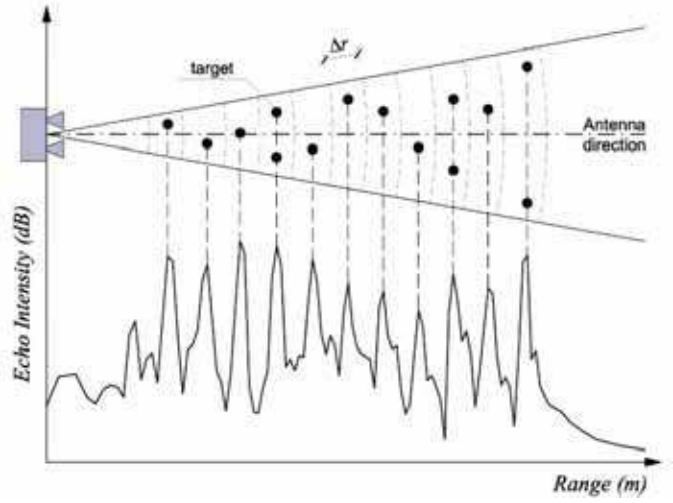

Fig. 3. Idealization of a radar image profile (range profile)

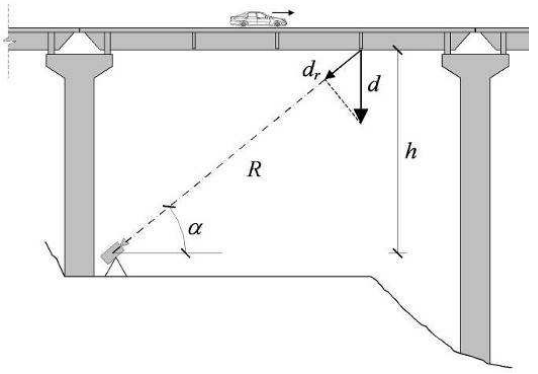

Fig. 4. Radial displacement vs. actual (i.e. vertical) displacement

2.2 The Interferometric technique

Once the range profile has been determined at uniform sampling intervals $\Delta t = 1/f_{sample}$, the displacement response of each range bin is evaluated by using the phase interferometry (Henderson & Lewis 1998); according to this technique, the displacement of a scattering

object is evaluated by comparing the phase information of the electromagnetic waves reflected by the object in different time instants.
Since two images obtained at different times exhibit phase differences, depending on the motion of the scatterers along the direction of wave propagation, the radial displacement d_r (i.e. the displacement along the radar line-of-sight) is simply computed from the phase shift $\Delta\vartheta$ as:

$$d_r = -\frac{\lambda}{4\pi}\Delta\vartheta \tag{7}$$

where λ is the wavelength of the electromagnetic signal.
It is worth underlining that the interferometric technique, represented by eq. (7), provides a measurement of the radial displacement of all the range bins of the structure illuminated by the antenna beam; hence, the evaluation of the actual displacement requires the knowledge of the direction of motion. For many bridges (simple or continuous spans, frame or truss bridges), the displacement under traffic loads can be assumed as vertical and it can be easily evaluated by making straightforward geometric projections, as shown in Fig. 4.

3. Description and technical characteristics of the microwave interferometer

The radar techniques described in the previous section have been implemented in an industrially engineered micro-wave interferometer by IDS (Ingegneria Dei Sistemi, Pisa, Italy); the new sensor, named IBIS-S (*I*mage *B*y *I*nterferometric *S*urvey of *S*tructures), consists of a sensor module, a control PC and a power supply unit (Fig. 5).
The sensor module is a coherent radar (i.e. a radar preserving the phase information of the received signal) generating, transmitting and receiving the electromagnetic signals to be processed in order to compute the displacement time-histories of the investigated structure. This unit, weighting 12 kg, includes two horn antennas for transmission and reception of the electromagnetic waves and is installed on a tripod equipped with a rotating head (Fig. 5), allowing the sensor to be orientated in the desired direction.

Fig. 5. View of the IBIS-S microwave interferometer

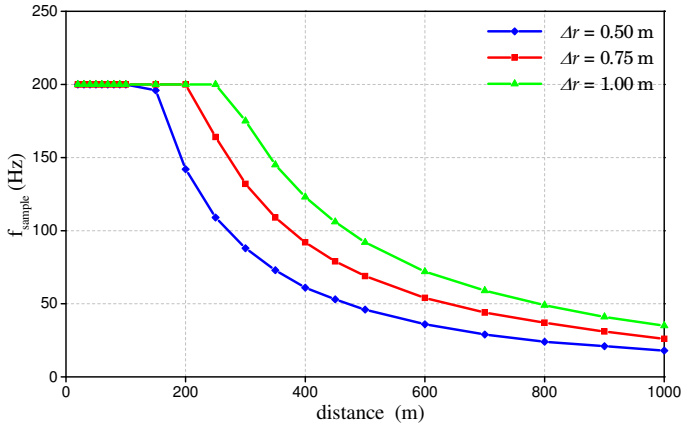

Fig. 6. Sampling rate vs. maximum distance for three different values of Δr

The radio-frequency section radiates at a central frequency of 16.75 GHz with a maximum bandwidth of 300 MHz; hence, the radar is classified as K_u-band, according to the standard radar-frequency letter-band nomenclature from IEEE Standard 521-1984.
The sensor unit is connected to the control PC by means of a standard USB 2.0 interface; the control PC is provided with a specific software for the management of the system and is used to configure the acquisition parameters, to manage and store the measurements and to show the displacements in real time.
The power supply unit, consisting of 12V battery packs, provides the power to the system for 5-6 hours.
The IBIS-S interferometric radar was designed to provide:

1. minimum range resolution Δr of 0.50 m, so that two targets can still be detected individually if their relative distance is greater than or equal to 0.50 m;
2. maximum sampling frequency of the scenario f_{sample} of 200 Hz, which is an excellent performance since the significant frequency content of displacement time-histories is generally in the frequency range 0–20 Hz for a civil engineering structure. In addition, sampling interval Δt=0.005 s is in principle well suitable to provide a good waveform definition of the acquired signals.

As a consequence of the radar techniques implemented in the sensor, the maximum operating distance depends on f_{sample} and Δr (see eq. 6). The dependence of sampling rate on the maximum distance is shown in Fig. 6, for three different distance resolutions. The inspection of Fig. 6 reveals that, for a range resolution of 0.5 m, the sampling rate drops off for distances greater than 150.0 m while, for a range resolution of 1.0 m, the sampling rate starts to decrease for distances greater than 300.0 m and reaches the value of 35 Hz for a range of 1000.0 m.

4. Accuracy and validation of the radar technique

4.1 Laboratory test

Unlike other non-contact techniques of deflection measurement, that are characterized by an accuracy generally ranging between 1.0-4.0 mm (image-based techniques) and 1.0 cm (GPS), sub-millimetric accuracy has in principle to be expected from the design specification on the

components of the microwave interferometer. This performance was verified in various laboratory tests, before using the radar in the field on full-scale structures. Among these tests, the free-vibration response of a simple mass-spring system was measured (Bernardini *et al.* 2007).

The test set-up was arranged by installing the mass-spring system, modified by adding a small and light passive radar reflector (corner reflector), in front of the radar sensor at a distance of 7.0 m. Fig. 7 shows a sketch of the test set-up and a photograph of the oscillator equipped with the corner reflector. The control PC of the sensor was configured to measure targets up to a distance of 50.0 m and with a scenario sampling frequency of 50 Hz.

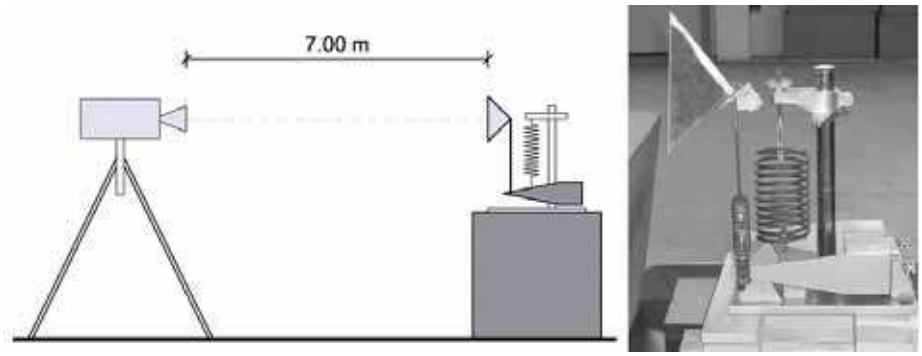

Fig. 7. Mass-spring system tested in laboratory and test set-up

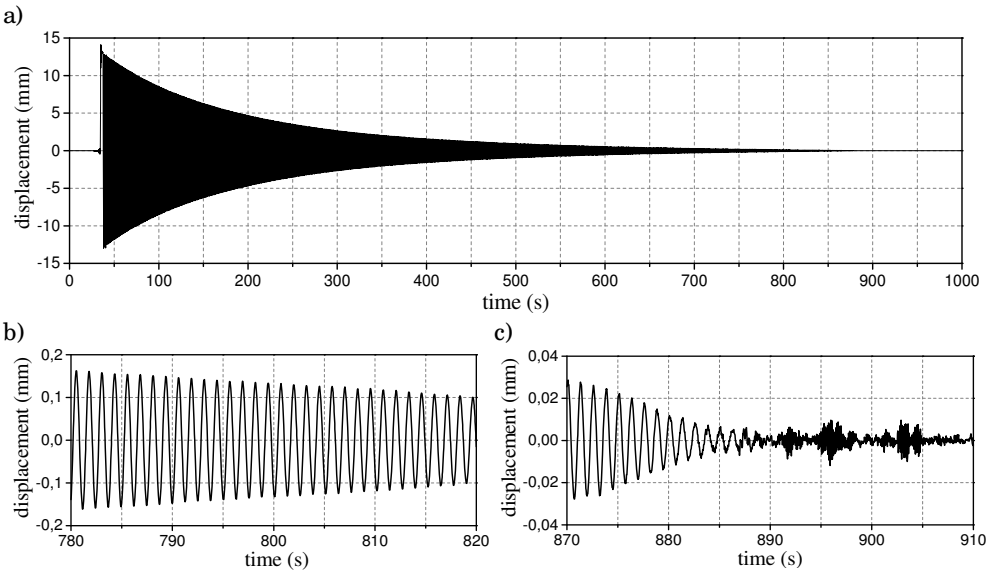

Fig. 8. a) Radar-based measurement of the displacement of a mass-spring system in laboratory test; b) zoom of the measured displacement in time interval 780–820 s; c) zoom of the measured displacement in time interval 870–910 s

Fig. 8a shows the free-damped displacement measured by the radar sensor in 1000 s of observation and the measured time-history corresponded perfectly to what expected for a lightly damped single-degree-of-freedom system. In order to better illustrate the characteristics of the measured response, Figs. 8b and 8c show temporal zooms of the displacement time-histories in the low-amplitude range. Fig. 8b clearly shows that the damped harmonic motion is very well described when its amplitude ranges between 0.1 and 0.2 mm. A similar performance appears in Fig. 8c, corresponding to the end of the free-damped motion: the measurement seems to exhibit excellent quality until the amplitude of the displacement exceeds 0.01–0.02 mm.

The inspection of Figs. 8a-c clearly highlights that – at least in a laboratory test and at a distance of 7.0 m – the accuracy of the sensor is better than 0.02 mm. It is worth underlining that other similar tests are currently in execution for distance ranging from 10.0 to 100.0 m.

4.2 Ambient vibration test of a reinforced concrete bridge

The radar equipment was first used on site during the ambient vibration test (AVT) of a reinforced concrete bridge crossing the river Adda (Gentile & Bernardini 2008), between the towns of Capriate and Trezzo (about 50 km north-east of Milan, Italy).

Plan and elevation of the bridge are shown in Fig. 9. The deck has a total length of 113.3 m and consists of two variable-depth balanced cantilevers (47.9 m long), connected by one simply-supported drop-in girder. Each balanced cantilever consists of a three-cell concrete box girder, while the central girder consists of a concrete slab supported by 4 girders and 3 cross-beams. The total width of the deck is 10.10 m.

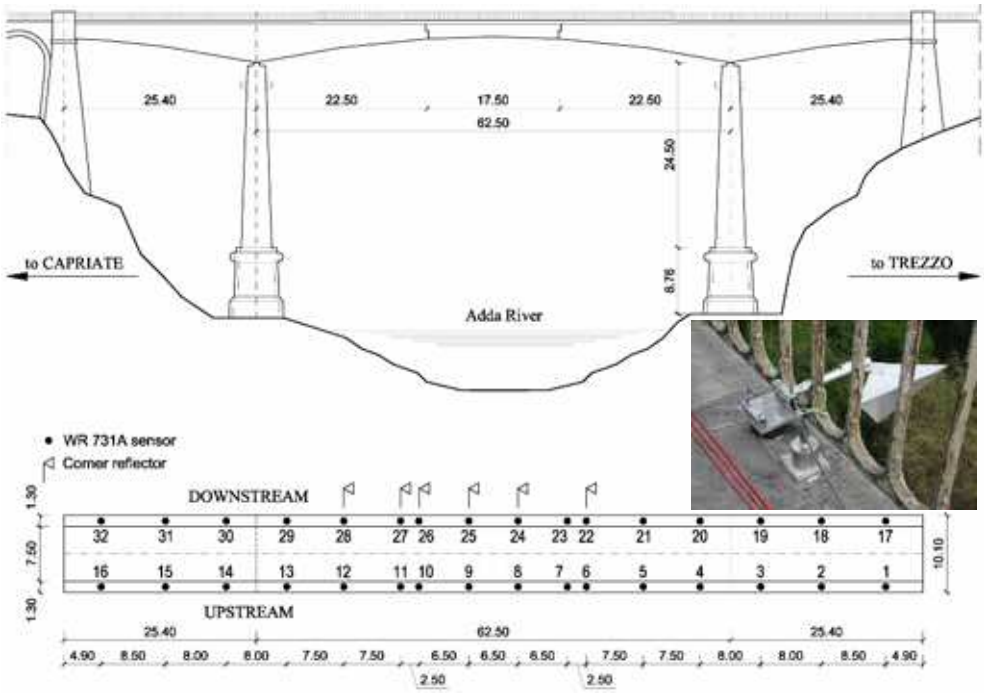

Fig. 9. Elevation and plan of the Capriate bridge, and sensor layout during the bridge tests

In this test, the ambient vibration response of the bridge was measured by simultaneously using the radar sensor and conventional accelerometers. In order to provide accurate comparison between the signals acquired from the different sensors, simple passive radar reflectors were placed as close as possible to the accelerometers (Fig. 9).
Two series of AVTs were carried out and the response of the bridge was measured at selected points using WR-731A sensors, each with a WR-P31 power unit/ amplifier. These sensors, allowing acceleration or velocity responses to be recorded, were used as conventional accelerometers in the first series of tests to identify the dynamic characteristics of the bridge; velocity time-histories were recorded during the second series of tests, when the microwave interferometer and the WR-731A sensors were simultaneously used.
The objective of the tests was two-fold. First, the agreement between the time-histories evaluated from the radar and the ones recorded by conventional sensors was extensively investigated (over a time window of 3000 s) in correspondence of several target surfaces (Fig. 9); more specifically, the velocity time-histories directly recorded by the WR 731A sensors were compared to the ones computed by deriving the displacements obtained by the IBIS-S sensor. Subsequently, resonant frequencies and mode shapes of the bridge, identified from the radar signals, were compared to the corresponding quantities estimated from the accelerometer's records.
An example of comparison between radar and conventional signals is given in Figs. 10a-b; the figures refer to the velocities simultaneously recorded at test points TP22 and TP27 over a short time period (12 s) and clearly show an excellent agreement between the data obtained from radar and conventional sensors. A similar agreement was obtained for all corner reflectors during 3000 s of simultaneously acquired time window, provided that the deflection response exceeds 0.01–0.02 mm.

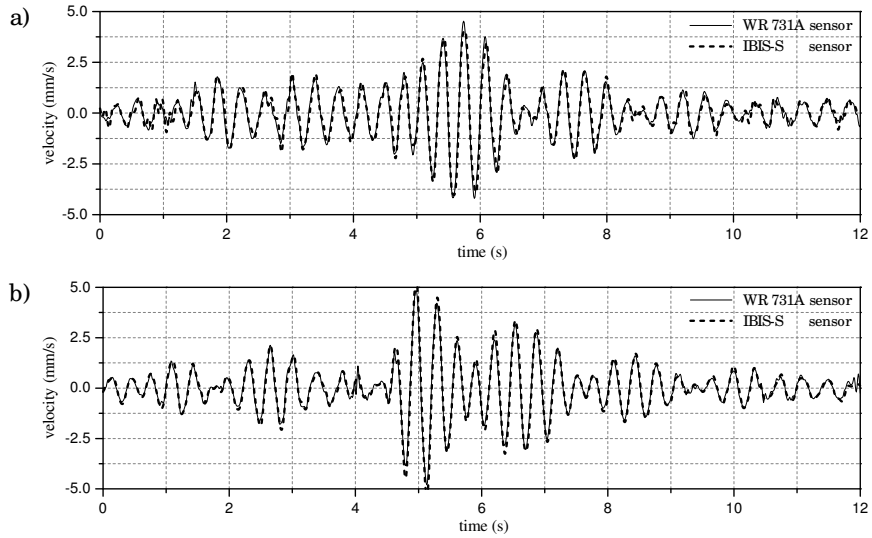

Fig. 10. Capriate bridge: comparison between the velocity time-histories collected by WR 731A and IBIS-S sensors at: a) TP22; b) TP27

As a consequence of the time-histories agreement, resonant frequencies and mode shapes provided by the radar sensor turned out to be as accurate as those obtained with traditional accelerometers (Gentile & Bernardini 2008), as shown in Fig. 11.
Finally, it is worth underlining that the microwave interferometer exhibits a remarkable stability in long term functioning on site (required for effective employment in AVT or continuous dynamic monitoring) and its use is relatively simple.

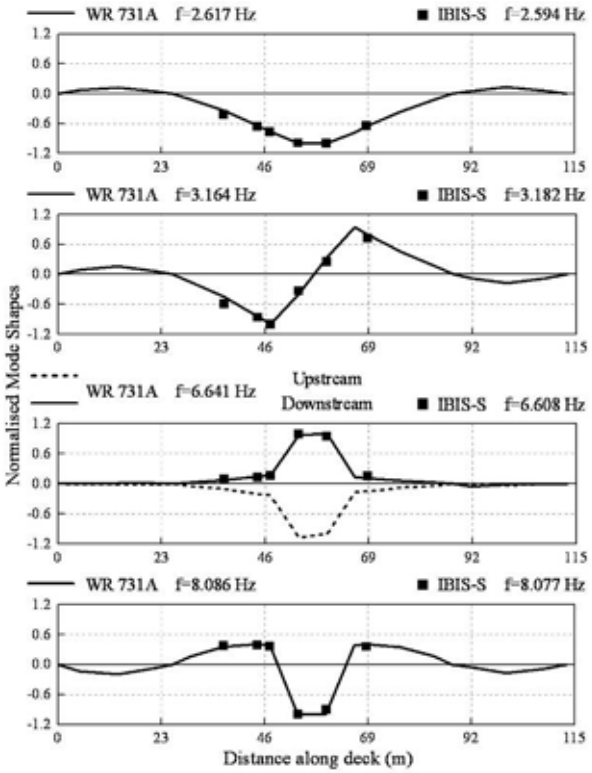

Fig. 11. Capriate bridge: comparison between natural frequencies and mode shapes identified from WR 731 and IBIS-S sensors data

4.3 Static test of a steel-composite bridge

In order to perform direct validation of the deflection measured by the radar and to assess the performance of the non-contact radar technique without the use of corner reflectors, extensive static tests were carried out on some spans of a steel-composite bridge. Steel and steel-composite bridges are much more reflective to electromagnetic waves than the concrete ones; furthermore, the deck generally includes a large number of corner zones, provided by the intersection of girders and cross-beams.
Since the static tests with the radar equipment were conducted taking profit of the simultaneous execution of standard reception tests of the investigated bridge, experimental data were collected by simultaneously using the radar technique and conventional techniques, with validation purposes.

The investigated bridge belongs to a motorway intersection recently completed in the neighbourhood of Forlanini Avenue, Milan, that is the main road linking the city centre to the city airport of Linate. The new infrastructure, shown in Fig. 12, includes two viaducts over-passing Forlanini Avenue.
The south-side viaduct is a continuous span steel-concrete composite bridge, consisting of 8 spans; the intermediate spans are generally 50.0 m long, while the end-spans are 38.0 m long, for a total length of 376.0 m. The structure consists of ladder beams with cantilevers; hence, the cross-section (Fig. 13) is characterised by two main longitudinal girders with transverse cross-beams, at a longitudinal spacing of 4.17 m. The cross-beams are extended beyond the girder to form cantilevers spanning 4.15 m. The girders are 2.55 m high while the floor beams are 1.00 m high. Girders and floor beams have wide flanges supporting a reinforced concrete slab, 25.0 cm thick. The total width of the deck is 18.0 m for three traffic lanes and two lateral emergency lanes.

Fig. 12. Aerial view of the new viaduct over Forlanini Avenue, Milan, Italy

a) b)

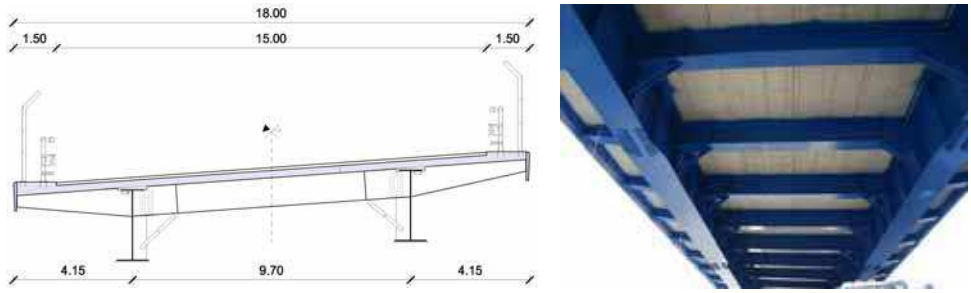

Fig. 13. a) Typical cross-section of the bridge over-passing Forlanini Avenue; b) Bottom view of the bridge deck

As it is usual in reception tests of new bridges, the focus of the test program was the measurement of vertical deflections of the bridge under live load. Vehicles of known weight were located at selected points of the viaduct and vertical deflections were measured at the centre of the girders of loaded spans by using traditional Linear Variable Differential Transformer (LVDT) Schaewitz extensometers.
The source of the live load for the test program was a series of 12 two-axle trucks, weighting between 415 kN and 440 kN. The test vehicles were placed according to four different

arrangements to provide four live load cases. For all live load configurations, the test vehicles were positioned to simultaneously load two spans of the viaduct and longitudinally with the rear axle centred on the mid-span (Fig. 14). Since the deck is characterized by a significant transverse slope (Fig. 13), the position of the vehicles was transversely non-centred between the two main girders in order to experimentally evaluate the torsion effects. (Fig. 14a).

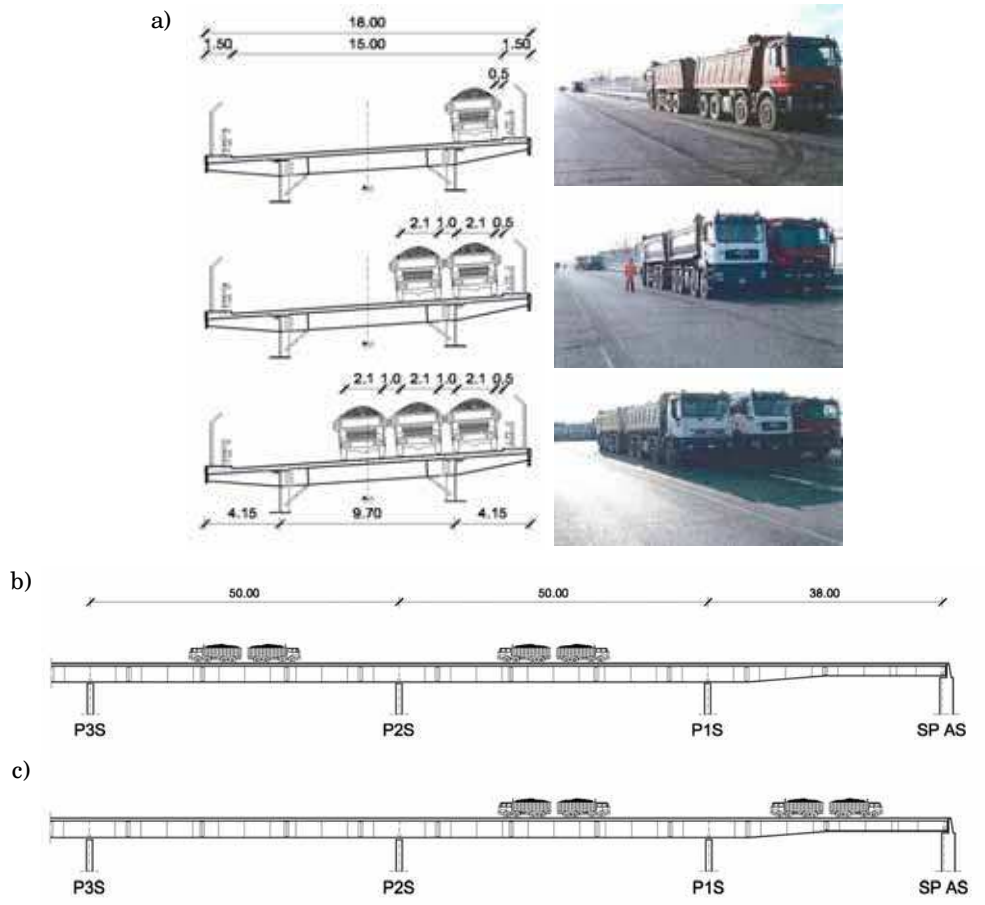

Fig. 14. Bridge over-passing Forlanini Avenue: a) transverse positioning of the test vehicles; b) longitudinal scheme of load condition LC1; c) longitudinal scheme of load condition LC2

The results of two load configurations will be presented and discussed in the following. These two load cases, shown in Fig. 14, are herein after referred to as LC1 (test vehicles loading the two spans between piers P3S and P1S on the west-side of the structure, Fig. 14b) and LC2 (test vehicle loading the two end spans on the west-side, Fig. 14c).

In all load conditions, the radar has been configured to measure targets up to a distance of 150.0 m, with a scenario sampling frequency of 10 Hz. Fig. 15 shows the position of the extensometers on span P2S-P3S and IBIS-S sensor during load configuration LC1. Since the

deck includes a large number of corner zones, provided by the intersection of girders and cross-beams, the exterior position of the microwave interferometer (Fig. 15) has to be preferred, in order to avoid the possible occurrence of multiple contributions to the same range bin coming from different reflective zones placed at the same distance from the radar (Gentile *et al.* 2008).

Fig. 16 shows the range profile of the scenario detected in LC1, projected along the longitudinal axis of the bridge. The analysis of the results provided by the microwave interferometer begins with the inspection of the range profile; this inspection, performed on site, allows to verify that the sensor positioning provides a correct image of the scenario. The radar image of Fig. 16 exhibits several peaks clearly marking the relative distance from the sensor of the transverse cross-beams reflecting the electromagnetic waves. It should be noticed that the peaks of Fig. 16 identify with excellent accuracy the cross-beams, provided that the distance between the radar and the axis of P3S pier (2.40 m, see Fig. 15) is properly accounted for.

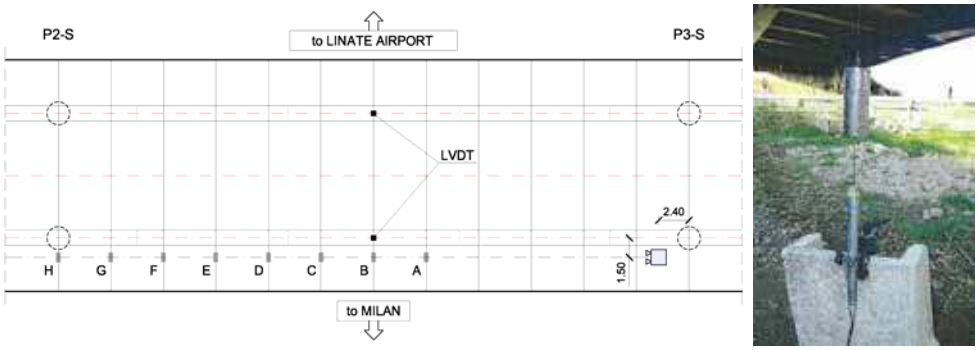

Fig. 15. Bridge over-passing Forlanini Avenue: radar and LVDT position in load condition LC1

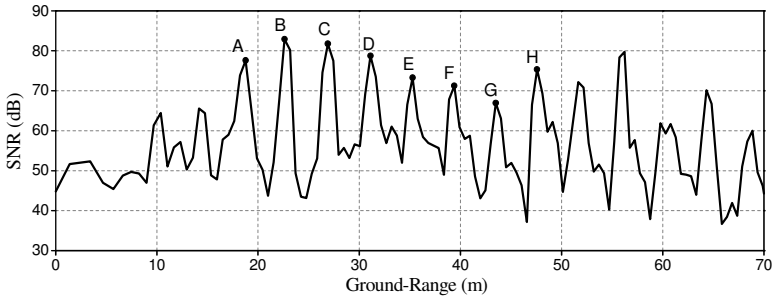

Fig. 16. Ground-Range profile in load condition LC1

It is further observed that the areas of the cross-beams corresponding to the peaks of Fig. 16 are in principle placed along the radar's line of sight (as it is schematically shown in Fig. 15).

Fig. 17 shows an example of displacement time-histories corresponding to different range bins and hence to different positions along the deck. It is observed that all deflections exhibit

similar evolution and the time windows corresponding to successive entrance and motion (150-400 s, 700-950 s and 1050-1250 s) of the test vehicles along the bridge are clearly identified in Fig. 17; in addition, as it has to be expected, deflection decreases from mid-span (curve B in Fig. 17) to pier (curve H in Fig. 17). Fig. 17 also compares the deflection obtained by the radar at mid-span (region B of Fig. 15) to the one directly measured by the neighbouring extensometer; it has to be noticed that the radar-based measurement slightly exceeds the conventional measurement, conceivably as a consequence of the torsion behaviour of the deck.

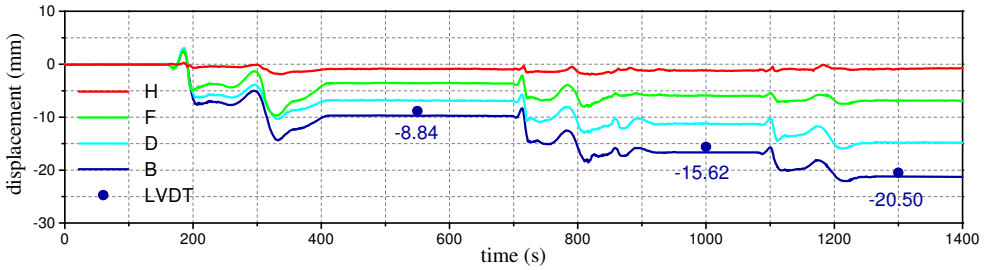

Fig. 17. Load Condition LC1: progress in time of the vertical displacements measured by the radar technique and comparison with the extensometer measurement

In load condition LC2, the radar position was moved as shown in Fig. 18, in order to have significant echo from all the transverse cantilevers and to obtain the deflected elastic curve of the whole span P1S-P2S. The corresponding range profile (Fig. 19) allows to clearly identify the cross-beams and confirms that all cantilevers of span P1S-P2S provide a sufficient echo.

Again the progress in time of the deflections measured by the radar clearly corresponds to the different phases of the load condition (Fig. 20) and good agreement was found between the results provided by radar and extensometer; in this case, as shown in Fig. 20, the difference between conventional and radar measurement is larger than in LC1 (Fig. 17), due to either the torsion behaviour of the deck or the slightly curved geometry of the investigated span.

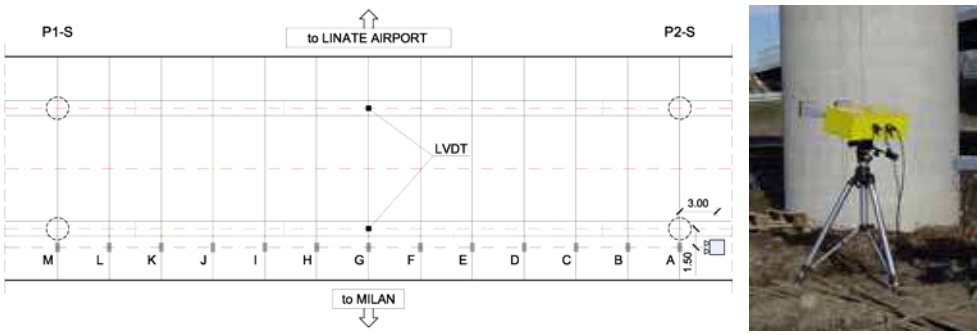

Fig. 18. Bridge over-passing Forlanini Avenue: radar and LVDT position in load condition LC2

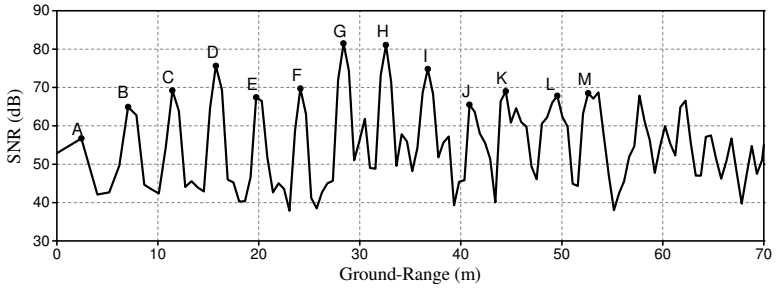

Fig. 19. Ground-Range profile in load condition LC2

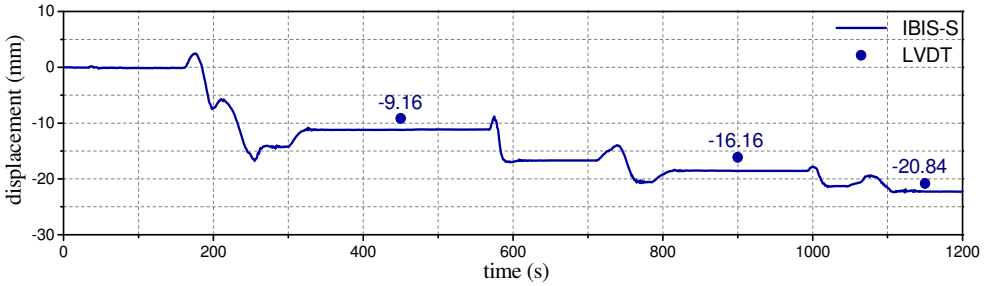

Fig. 20. Load Condition LC2: progress in time of the vertical displacements measured by the radar technique and comparison with the extensometer measurement

5. Dynamic measurements on cable stays

The application of the radar technique to the measurement of cable vibrations seems especially promising in order to perform systematic dynamic assessment of stay cables in a simple and quick way.

It is worth underlining that dynamic measurements on stay cables are generally aimed at: (1) evaluating the amplitude of cable vibrations; (2) identifying the local natural frequencies and damping ratios; (3) evaluating the cable forces and monitoring the changes in these forces over time; (4) investigating potential fatigue problems in the cables.

When a linear correlation exists between the mode order and the corresponding natural frequency of a stay cable (Robert *et al.* 1991), the tension force can be obtained from cable's natural frequencies using the taut string theory (see e.g. Irvine 1981, Caetano 2007). For the tension members that deviate from a taut string, still the cable forces can be predicted by using the identified natural frequencies with reference to more advanced formulations (accounting for the effects of both the sag and the bending stiffness on the dynamic behaviour of cables, see e.g. Casas 1994, Mehrabi & Tabatabai 1998). Subsequently, the knowledge of cable forces is used to check the correct distribution of the internal forces in the bridge at the end of construction, while monitoring the possible changes in stay cable forces over time may provide an efficient method for Structural Health Monitoring. For example, a significant drop in the tension force of a cable with simultaneous increases in the forces of the neighbouring cables may be a clear indication of a loss of cross section (or slippage at the anchorage) for the cable exhibiting the force drop.

When compared to other techniques of remote sensing, the microwave interferometry exhibits several advantages:

1. low power transmitted;
2. higher accuracy;
3. possibility of simultaneously measuring the dynamic response of all cables belonging to an array.

In addition, the possible issues that may occur in the application of the radar technique to bridges and large structures practically cannot affect the radar the survey of an array of cables; peculiarly:

a. the typical position of the sensor in the survey of an array of cables is inclined upward, as schematically shown in Fig. 21a; hence, the only targets encountered along the path of the electromagnetic waves are the stays itself so that 1-D imaging capability is perfectly adequate to the test scenario;
b. it can assumed that the in-plane motion of the cable is orthogonal to its axis, so that the actual deflection d can be expressed as:

$$d = \frac{d_r}{\cos[\pi/2 - (\alpha_c + \alpha_s)]} \tag{8}$$

where α_c and α_s are the slope of the cable and of the sensor, respectively (Fig. 21a). In other, words, the prior knowledge of the direction of motion is available for cable systems so that it is possible to evaluate the actual displacement from the radial one.

Furthermore, since it is quite easy to predict the scenario under the radar beam (Fig. 21b), the inspection of the range profile allows to quickly verify that the sensor positioning provides a correct image of the scenario.

The accuracy and operational simplicity of the radar techniques in vibration survey of stay-cables arrays has been to date verified on two cable-stayed bridges (Gentile *et al.* 2008, Gentile 2009): some results obtained on the cable-stayed bridge crossing the Oglio river between the municipalities of Bordolano and Quinzano (northern Italy) are herein after presented and discussed.

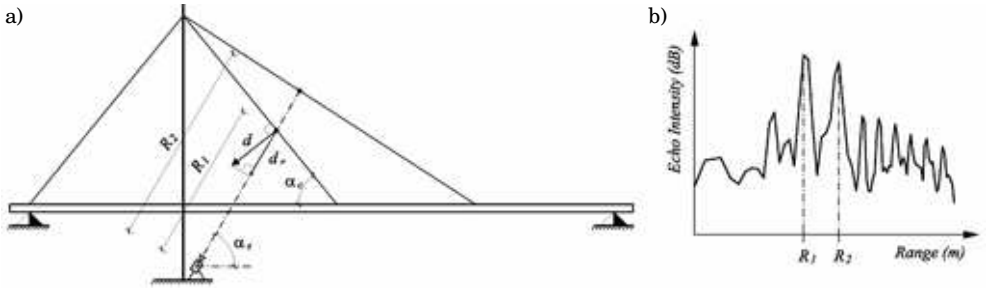

Fig. 21. a) Radial displacement versus actual (in-plane) displacement of a stay cable; b) Typical range profile expected for an array including two cables

The dynamic characteristics of the investigated cable-stayed bridge were well-known since ambient vibration measurements were carried out on the bridge in Spring 2004 by the Vibration Laboratory of L'Aquila University (Benedettini & Gentile 2008), using Sprengnether servo-accelerometers. During this test, 10 global modes of the bridge were

identified in the frequency range 0–10 Hz and also the dynamic response of one cable (S_{2U} in Fig. 22) was recorded.

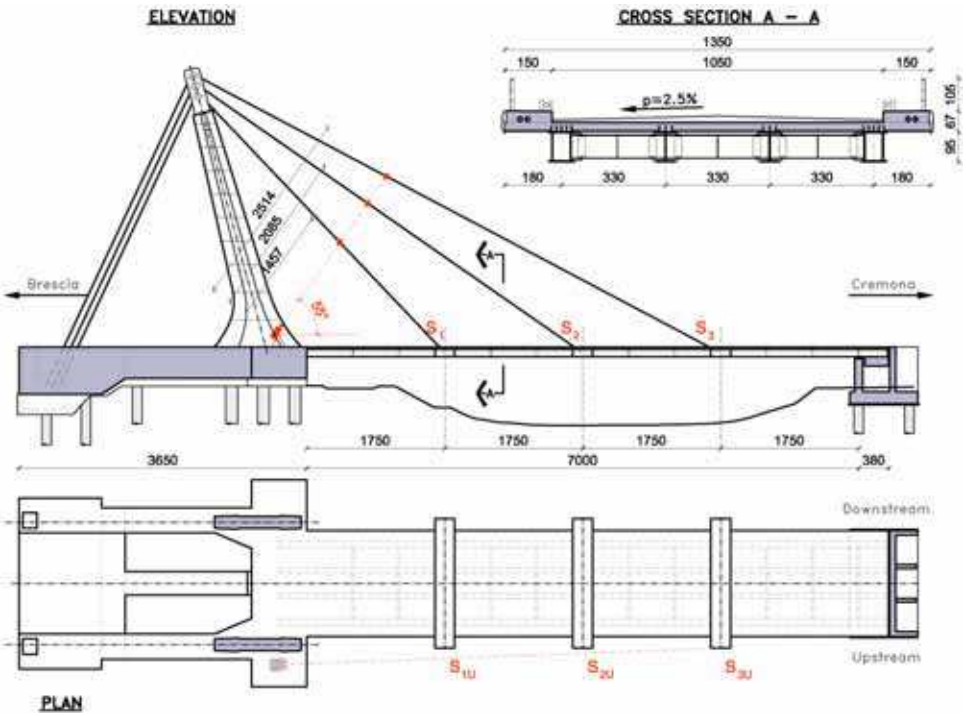

Fig. 22. Elevation, plan and cross-section of the investigated cable-stayed bridge. Position of the radar sensor during the test of stay cables S_{1U}, S_{2U} and S_{3U} (upstream side)

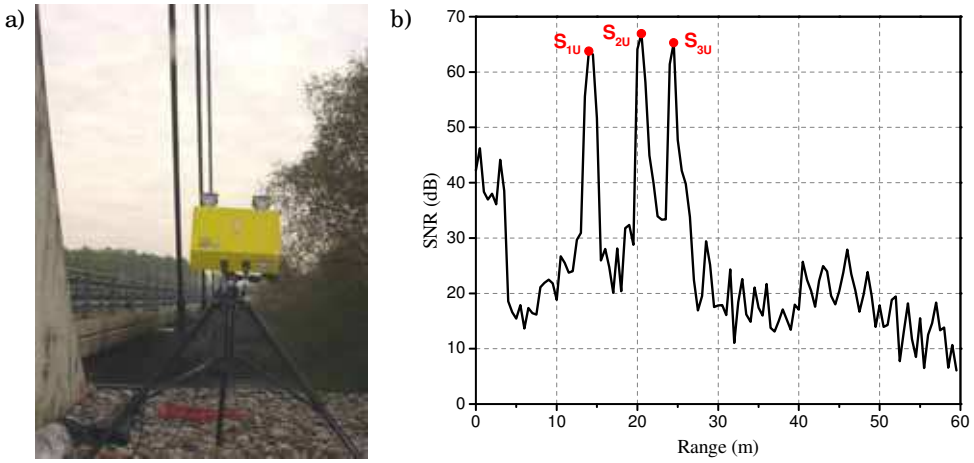

Fig. 23. a) View of the radar position during the test of stay cables S_{1U}-S_{3U} (upstream side); b) Range profile of the test scenario

Elevation and plan views of the bridge and typical cross-section are presented in Fig. 22. The cross-section (Fig. 22) consists of 4 steel girders framed by floor beams; girders and floor beams are all composite with a 30.0 cm concrete slab. The steel girders are 95 cm high, with the outer girders (spaced 9.90 m centre to centre) being of box section while the inner ones are wide flange sections. The girders are framed by floor beams 5.83 m spaced; the floor beams providing the anchorage of the stays are of box section while the other ones are wide flange sections (Fig. 22). The total width of the deck is 13.50 m for two traffic lanes and two pedestrian walkways; the suspended span is 70.0 m long. The cast-in-place concrete towers are 35.65 m high and each consists of an inclined, varying width, concrete leg bearing an upper steel device providing the anchorage for the stay cables.

In the test of array including cables S_{1U}-S_{8U} on the upstream side (Fig. 22), the radar sensor was placed on the basement of the upstream-side tower, as shown in Figs. 22 and 23a. The range profile of the test scenario is presented in Fig. 23b and exhibits three well defined peaks, clearly identifying the position in range of the cables.

3000 s of radar data were acquired at a rate of 200 Hz. Figs. 24a-b show the auto-spectral densities (ASD) associated to the ambient response of stay cables S_{1U} and S_{8U}, respectively. The ASD plots in Fig. 24 are a synthesis of the frequency content present on each cable and allowed the identification of several local resonant frequencies, marked with the vertical lines, in the frequency range of analysis (0–25 Hz).

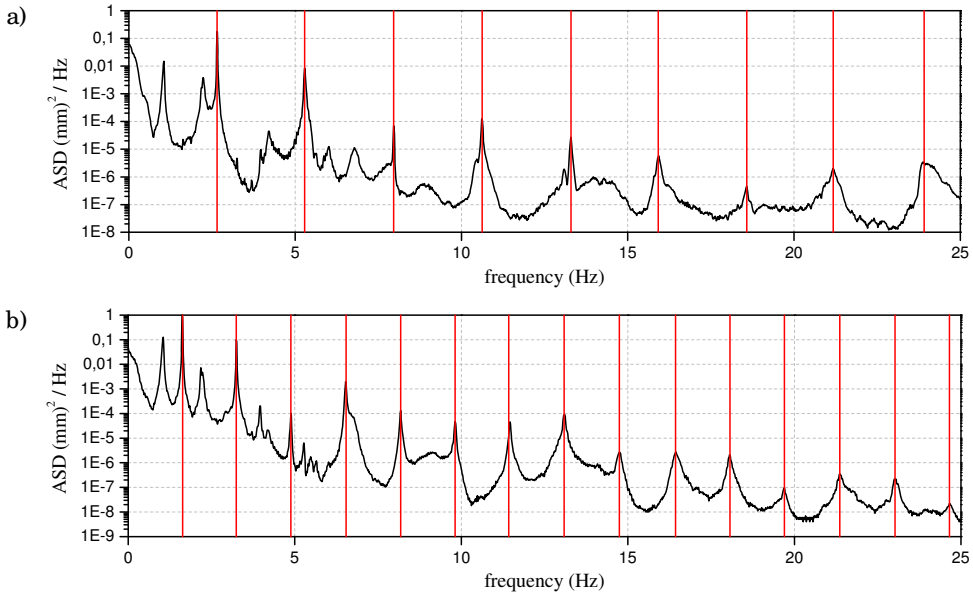

Fig. 24. Auto-spectra of the displacement data measured by the radar on cables: a) S_{1U}; b) S_{8U}

Furthermore, Fig. 25 presents a direct comparison between: (1) the auto-spectrum of the acceleration measured on stay cable S_{2U} by a conventional accelerometer in the test of Spring 2004 and (2) the auto-spectrum of the acceleration obtained from the radar sensor (and computed by deriving the displacement data).

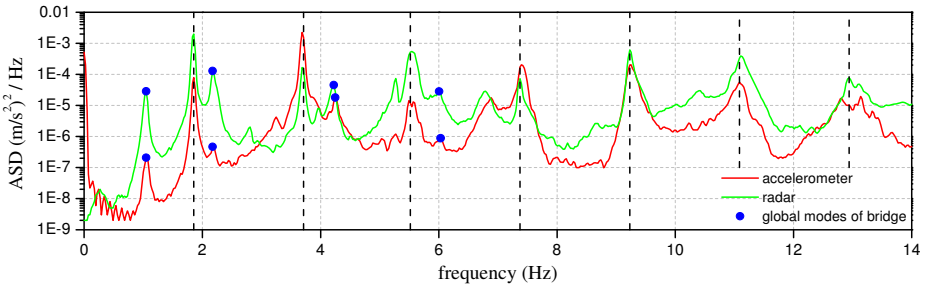

Fig. 25. Comparison between the auto-spectra of the acceleration data of cable S_{2U} obtained from conventional and radar sensor

From the inspection of the spectral plots in Figs. 24a-b and 25, one can observe that:

1. the response of cables S_{1U} and S_{3U} (Fig. 24) in the frequency range 0-25 Hz is characterized by several equally spaced and well-defined peaks. Since a linear correlation exists between the mode order and the corresponding natural frequency of the cables, the tension forces computed from cable's natural frequencies using the taut string theory (see e.g. Irvine 1981, Casas 1994, Caetano 2007) turned out to be practically equal to the design values;
2. the values of the first seven natural frequencies of stay cable S_{2U}, identified on the basis of the auto-spectra obtained using conventional and radar measurement systems are virtually coincident (1.84, 3.70, 5.53, 7.37, 9.24. 11.1 and 12.93 in Fig. 25);
3. some global natural frequencies of the bridge (corresponding to peaks of the ASDs placed at 1.06, 2.18, 4.25 and 6.03 Hz) are also apparent in Figs. 24-25 and are equal to the ones identified by (Benedettini & Gentile 2008) in the AVT of the bridge.

6. Conclusions

An innovative radar sensor, developed for remote (non contact) measurements of deflections on bridges and large structures in both static and dynamic conditions, has been presented. The new sensor exhibits various operational advantages with respect to contact sensors and, at the same time, provides a direct measurement of displacement, which is of utmost importance in the in-service monitoring of large structures. Furthermore, based on the design specifications of the system components, the displacements sensitivity is expected to range between 1/ 100 and 1/ 10 mm.

The accuracy of the sensor has been evaluated in laboratory tests carried out on a simple mass-spring system; the free-vibration tests carried out on the oscillator confirm that the displacement sensitivity is better than 2/ 100 mm; in addition, the laboratory tests indicated both an excellent quality for the measured displacements and a good operating stability of the equipment.

The use of the radar interferometer in static and dynamic tests of two full-scale bridges exhibited excellent stability, when employed on site for long time intervals.

Based on the analysis of the results of the above tests, including (a) the inspection of the displacement responses obtained from the radar sensor and (b) the comparison with the data recorded by conventional sensors (LVDT extensometers and accelerometers), the following conclusions can be drawn:

1. the radar-based deflection measurements obtained during live-load static tests seem as accurate as that obtained with the conventional extensometers;
2. the velocity time-histories evaluated from the radar sensor (and obtained by deriving the displacements) generally exhibit very good agreement with the ones recorded by conventional sensors;
3. an excellent agreement was found between the modal parameters (resonant frequencies and mode shapes) identified from radar data and from data obtained with conventional accelerometers.

Furthermore, the radar technique turned out to be especially suitable to vibration survey of stay cables since it allows to simultaneously measure the dynamic response of several stay-cables and provides measurements of high level of accuracy in terms of identification of natural frequencies.

Notwithstanding the good results obtained by using the microwave sensor, it has to be recalled that two main issues may occur in the application of radar techniques to bridges and large structure:

a. as a consequence of the 1-D imaging capabilities of the radar sensor, measurement errors may arise when different points of a structure are placed at the same distance from the radar;
b. the radar provides a measurement of the variation of the target position along the sensor's line of sight (i.e. the radial displacement); hence, the evaluation of the actual displacement requires the prior knowledge of the direction of motion.

7. Acknowledgements

The author would like to acknowledge: (1) the support provided by the Italian Ministry of University and Research (MIUR), within a National Project funded in 2006, and by IDS (Ingegneria Dei Sistemi, Pisa, Italy), owner and developer of the microwave interferometer used in the tests; (2) Dr. Giulia Bernardini (IDS) and the Local Administrations owners of the tested bridges: without their involvement and co-operation, this research would not have been possible; (3) Prof. Francesco Benedettini (L'Aquila University) for the kind concession of the data recorded in Spring 2004 and presented in Fig. 25; (4) the help provided by Marco Antico, Marco Cucchi and Dr. Nicola Gallino (Laboratory of Vibrations and Dynamic Monitoring of Structures, Politecnico di Milano) in conducting the field tests.

8. References

Benedettini, F. & Gentile, C. (2008): F.E. modelling of a cable-stayed bridge based on operational modal analysis, *Proceedings of 26th Int. Modal Analysis Conf.* (IMAC-XXVI).

Bernardini, G. et al. (2007). Microwave interferometer for ambient vibration measurements on civil engineering structures: 1. Principles of the radar technique and laboratory tests, *Proceedings of Int. Conf. on Experimental Vibration Analysis of Civil Engineering Structures* (EVACES'07), 143-152.

Caetano, E. (2007). *Cable vibrations in cable stayed bridges*, SED 9, IABSE.

Casas, J.R. (1994). A combined method for measuring cable forces: the cable-stayed Alamillo Bridge, Spain, *Structural Engineering International* , 4(4), 235–240.

Cunha A. & Caetano E. (1999). Dynamic measurements on stay cables of cable-stayed bridges using an interferometry laser system, *Experimental Techniques*, 23(3), 38-43.

Farrar, C.R., Darling, T.W., Migliori, A. & Baker, W.E. (1999). Microwave interferometers for non-contact vibration measurements on large structures, *Mech. Syst. Signal Process.*, 13(2), 241-253.

Farrar, C.R. & Cone, K.M., (1995). Vibration testing of the I-40 bridge before and after the introduction of damage, *Proceedings of 13th Int. Modal Analysis Conference* (IMAC-XIII).

Gentile, C. & Bernardini, G. (2008). Output-only modal identification of a reinforced concrete bridge from radar-based measurements, *NDT&E International*, 41(7), 544-553.

Gentile, C., Bernardini, G. & Ricci, P.P. (2008). Operational modal analysis of a cable-stayed bridge from conventional and radar-based measurements, *Proc. Eurodyn 2008*.

Gentile, C. (2009). Radar-based measurement of deflections on bridges and large structures: advantages, limitations and possible applications, *Proc. SMART'09*.

Irvine, M. (1981). *Cable Structures*, MIT Press.

Henderson, F.M. & Lewis, A.J (Eds.) (1998). *Manual of Remote Sensing. Principles and Applications of Imaging Radar*, Wiley & Sons, 3rd Ed.

Kaito, K., Abe, M. & Fujino, Y. (2005). Development of a non-contact scanning vibration measurement system for real-scale structures, *Structure & Infrastructure Engng*. 1(3), 189-205.

Lee, J.J. & Shinozuka, M. (2006). A vision-based system for remote sensing of bridge displacement. *NDT&E International*, 39(5), 425-431.

Marple, S.L. Jr. (1987). *Digital spectral analysis with applications*, Prentice-Hall.

Mehrabi, A.B. & Tabatabai, H. (1998). Unified finite difference formulation for free vibration of cables. *J. Structural Engineering*, ASCE, 124(11), 1313-1322.

Meng, X., Dodson, A.H. & Roberts, G.W. (2007). Detecting bridge dynamics with GPS and triaxial accelerometers, *Engineering Structures*, 29(11), 3178-3184.

Nickitopoulou, A., Protopsalti, K. & Stiros, S. (2006). Monitoring dynamic and quasi-static deformations of large flexible engineering structures with GPS: Accuracy, limitations and promises, *Engineering Structures*, 28(10), 1471-1482.

Pieraccini, M. et al. (2004). Highspeed CW step-frequency coherent radar for dynamic monitoring of civil engineering structures, *Electron. Lett.*, 40(14), 907-908.

Robert, J., Bruhat, D., & Gervais, J.P. (1991). Mesure de la tension de câbles par méthode vibratoire, *Laboratoire des Ponts et Chausseés*, 173(3), 109-114.

Silva, S., Bateira, J. & Caetano, E. (2007). Development of a vision system for vibration analysis, *Proceedings of Int. Conf. on Experimental Vibration Analysis of Civil Engineering Structures* (EVACES'07), 113-121.

Skolnik, M.I. (Ed.) (1990). *Radar Handbook*, McGraw-Hill.

Wehner, D.R. (1995). *High-resolution radar* , 2nd Ed., Norwood, MA: Artech House.

Radar Technology

Edited by Guy Kouemou

ISBN 978-953-307-029-2
Hard cover, 410 pages
Publisher InTech
Published online 01, January, 2010
Published in print edition January, 2010

In this book “Radar Technology”, the chapters are divided into four main topic areas: Topic area 1: “Radar Systems” consists of chapters which treat whole radar systems, environment and target functional chain. Topic area 2: “Radar Applications” shows various applications of radar systems, including meteorological radars, ground penetrating radars and glaciology. Topic area 3: “Radar Functional Chain and Signal Processing” describes several aspects of the radar signal processing. From parameter extraction, target detection over tracking and classification technologies. Topic area 4: “Radar Subsystems and Components” consists of design technology of radar subsystem components like antenna design or waveform design.

INTECH
open science | open minds

InTech Europe
University Campus STeP Ri
Slavka Krautzeka 83/A
51000 Rijeka, Croatia
Phone: +385 (51) 770 447
Fax: +385 (51) 686 166
www.intechopen.com

InTech China
Unit 405, Office Block, Hotel Equatorial Shanghai
No.65, Yan An Road (West), Shanghai, 200040, China
中国上海市延安西路65号上海国际贵都大饭店办公楼405单元
Phone: +86-21-62489820
Fax: +86-21-62489821